Microtubule plus end–associated CLIP-170 initiates HSV-1 retrograde transport in primary human cells

Vladimir Jovasevic,[1] Mojgan H. Naghavi,[1,2] and Derek Walsh[1,3]

[1]Department of Microbiology-Immunology, Feinberg School of Medicine, Northwestern University, Chicago, IL 60611
[2]Department of Biochemistry and Molecular Biophysics, College of Physicians and Surgeons, Columbia University, New York, NY 10032
[3]Department of Microbiology, School of Medicine, New York University, New York, NY 10016

Dynamic microtubules (MTs) continuously explore the intracellular environment and, through specialized plus end–tracking proteins (+TIPs), engage a variety of targets. However, the nature of cargoes that require +TIP-mediated capture for their movement on MTs remains poorly understood. Using RNA interference and dominant-negative approaches, combined with live cell imaging, we show that herpes simplex virus particles that have entered primary human cells exploit a +TIP complex comprising end-binding protein 1 (EB1), cytoplasmic linker protein 170 (CLIP-170), and dynactin-1 (DCTN1) to initiate retrograde transport. Depletion of these +TIPs completely blocked post-entry long-range transport of virus particles and suppressed infection ∼5,000-fold, whereas transferrin uptake, early endosome organization, and dynein-dependent movement of lysosomes and mitochondria remained unaffected. These findings provide the first insights into the earliest stages of viral engagement of MTs through specific +TIPs, akin to receptors, with therapeutic implications, and identify herpesvirus particles as one of a very limited number of cargoes absolutely dependent on CLIP-170–mediated capture to initiate transport in primary human cells.

Introduction

Intracellular movement of cargoes over long distances requires directed transport by motor proteins along microtubules (MTs). Generally, retrograde transport is mediated by the inward-directed motor dynein, whereas anterograde movement is mediated by kinesins (Kardon and Vale, 2009; Dodding and Way, 2011; Vallee et al., 2012). MTs themselves consist of α/β-tubulin heteropolymers that form polarized filaments whose minus ends nucleate at a MT organizing center, whereas their plus ends radiate outward, forming filaments that dynamically grow and shrink. This dynamic nature enables continuous environmental sensing through a process of "search and capture" (Gundersen, 2002). In response to specific cues, subsets of MTs can become stabilized, often through capture of dynamic MT plus ends at specific sites just beneath the plasma membrane (Gundersen, 2002). Stable MTs acquire distinguishing posttranslational modifications, including acetylation and detyrosination of tubulin subunits, and act as specialized tracks for vesicle trafficking (Gundersen, 2002). MT dynamics and stability are controlled by an array of specialized plus end–tracking proteins (+TIPs; Jiang and Akhmanova, 2011). Among these, the end-binding protein EB1 specifically recognizes the growing plus ends of dynamic MTs (Jiang and Akhmanova, 2011). Although EB1 can directly influence MT growth, it also plays a central role in MT regulation by recruiting other +TIPs to MT plus ends. Indeed, although many +TIPs can bind MTs, their specific accumulation at MT plus ends requires EB1 (Honnappa et al., 2009; Jiang and Akhmanova, 2011). +TIPs also function in the interaction of MTs with targets such as the cell cortex, organelles, and cargoes (Gundersen, 2002; Jiang and Akhmanova, 2011). However, as discussed later, the nature of cargoes captured by specific +TIPs to initiate their transport and the underlying mechanisms remain unclear.

As intracellular parasites, viruses represent an intriguing form of pathogenic cargo that are reliant on host transport networks to move to and from their subcellular sites of replication. Many initially exploit short-range actin-mediated transport at the periphery followed by long-range MT-based movement within the infected cell (Radtke et al., 2006; Dodding and Way, 2011). Indeed, many viruses physically associate with MT motors and adapters and have evolved to manipulate MT organization (Radtke et al., 2006; Dodding and Way, 2011). This includes herpes simplex virus type 1 (HSV-1), a widespread human pathogen that establishes life-long infections resulting in recurrent cold sores, corneal blindness, and encephalopathy (Roizman et al., 2007). However, although it has long been established that MT-depolymerizing or -stabilizing agents affect

Correspondence to Derek Walsh: derek.walsh@northwestern.edu; or Mojgan H. Naghavi: mojgan.naghavi@northwestern.edu

Abbreviations used in this paper: ANOVA, analysis of variance; DIC, dynein intermediate chain; fps, frame per second; hpi, hour post infection; IE, immediate early; IF, immunofluorescence; MT, microtubule; NHDF, normal human dermal fibroblast; qRT-PCR, quantitative real-time PCR; +TIP, plus end–tracking protein; WB, Western blot.

The Rockefeller University Press $30.00
J. Cell Biol. Vol. 211 No. 2 323–337
www.jcb.org/cgi/doi/10.1083/jcb.201505123

the establishment of infection (Kristensson et al., 1986; Sodeik et al., 1997; Mabit et al., 2002; Radtke et al., 2006; Dodding and Way, 2011), the nature of MT filaments involved and the underlying mechanisms by which viruses initially engage MTs remain unknown. Here, using RNAi and dominant-negative approaches, we uncover how HSV-1 particles that have entered cells exploit a dynamic MT plus end complex comprising EB1, cytoplasmic linker protein 170 (CLIP-170), and dynactin-1 (DCTN1). Furthermore, we illustrate how virus particles, unlike numerous host cargoes, exhibit a near absolute dependence on this specialized capture mechanism to initiate retrograde transport and infection in primary human cells.

Results

HSV-1 exploits dynamic MT filaments during early infection

Although HSV-1 induces and exploits stable MTs to promote egress and spread of new virus particles (Elliott and O'Hare, 1998; Naghavi et al., 2013), the potential role of stable MTs in early infection remains unknown. To establish whether HSV-1 affected MT stability early in infection, primary normal human dermal fibroblasts (NHDFs) were mock infected or infected with HSV-1 at MOI 20. Western blot (WB) analysis of cell lysates revealed that HSV-1 did not detectably alter acetylated tubulin (Ac-tubulin) levels over the first 3 h post infection (hpi), in stark contrast to the robust acetylation induced by 24 hpi (Fig. 1 A). To determine whether HSV-1 might exhibit preferential localization toward existing stable MTs, NHDFs were infected as described above and analyzed by immunofluorescence (IF). HSV-1 particles were stained using a monoclonal antibody against the capsid protein ICP5, whereas anti–Ac-tubulin antibody was used to stain stable MTs (Ac-MTs). Imaging revealed that viral particles were scattered throughout the cytoplasm at 1 hpi but became detectable at the nuclear periphery by 2 hpi (Fig. 1 B). By 3 hpi, nuclei of most cells became heavily stained for ICP5 as viral particles reached the nucleus (Fig. 1 B), in line with kinetics in other cell types (Sodeik et al., 1997). Furthermore, images revealed that Ac-MT levels and organization were not detectably altered by infection, and capsids did not exhibit notable colocalization with Ac-MTs that would suggest their specific use for viral transport (Fig. 1 B and Fig. S1). To test whether virus particles localized to dynamic MTs, infected cells were fixed and stained using antibodies that distinguish stable versus dynamic filaments; stable Ac-MTs were stained using anti–Ac-tubulin antibody, whereas dynamic MTs were visualized using antityrosinated tubulin antibody (Tyr-MTs; Naghavi et al., 2013). Confocal microscopy revealed that virus particles, detected using anti-ICP5 antibody, localized to Tyr-MTs that contained little or no Ac-tubulin and did not localize to filaments staining heavily for Ac-tubulin (Fig. 1 C). Overall, these findings demonstrated that HSV-1 neither induced nor colocalized with stable MTs during early infection and pointed to potential roles for dynamic MTs.

EB1 and CLIP-170 facilitate early post-entry stages of HSV-1 infection

To initially test whether +TIPs that associate with dynamic MTs contributed to HSV-1 infection, the effect of depleting EB1 was examined. NHDFs were treated with control nontargeting or EB1 siRNAs and then infected for 16 h at MOI 5 with HSV-1 expressing a GFP-tagged late protein, Us11 (HSV-1–GFP-Us11). Microscopy revealed that, compared with control siRNA, two independent EB1 siRNAs potently suppressed GFP-Us11 fluorescence signal and HSV-1–induced cytopathic effect in cultures (Fig. 2 A). The morphology of EB1-depleted cells suggested that this was not a result of effects on cell viability (Fig. 2 A), and further evidence for this is presented below. The reduction in GFP-Us11 levels provided functional evidence that dynamic MTs and +TIPs were required for HSV-1 infection. To test this further, the contribution of EB1 or CLIP-170, an EB1-binding +TIP that promotes MT growth and linkage to targets (Galjart, 2005), to production of infectious virus was examined. NHDFs were treated with control, EB1, or CLIP-170 siRNAs and then infected at MOI 5 for 16 h with either HSV-1–GFP-Us11 (Patton strain) or wild-type HSV-1 (strain F). Strikingly, NHDFs depleted of either EB1 or CLIP-170 were found to produce ∼5,000-fold less virus than control cultures for both virus strains tested (Fig. 2 B). WB analysis confirmed target depletion by each siRNA, whereas the levels of cleaved PARP-1, an apoptosis indicator, were found to be unchanged in either EB1- or CLIP-170–depleted infected cells compared with controls (Fig. 2 C), further demonstrating no adverse effects of +TIP depletion on cell viability.

To begin determining the stage of infection being affected, the expression of different kinetic classes of viral gene products was examined. HSV-1 gene expression begins with five immediate early (IE) genes followed by expression of early and then late genes (Roizman et al., 2007). Samples of siRNA-treated NHDFs infected at MOI 5 for 16 h were analyzed by WB for infected cell proteins ICP0, ICP4, and ICP22, representing key IE gene products as well as late viral structural proteins. Results showed that independent siRNAs against EB1 or CLIP-170 not only inhibited production of viral structural proteins, but also potently blocked the accumulation of IE proteins (Fig. 2 C). The degree to which viral protein production was suppressed directly correlated with the degree of EB1 or CLIP-170 depletion achieved with each siRNA tested. As discussed later, although CLIP-170 can bind tubulin, EB1 mediates its specific accumulation and function at MT plus ends in many cell types (Jiang and Akhmanova, 2011). To test this in NHDFs, the localization of these factors was examined in siRNA-treated cultures. In control samples, EB1 and CLIP-170 colocalized in comet-like staining patterns at MT plus ends (Fig. 2 D). CLIP-170 was also observed in what has been described previously as "patches" along the MT lattice (Rickard and Kreis, 1990; Pierre et al., 1992), which did not colocalize with EB1. In CLIP-170–depleted NHDFs, EB1 staining was unaffected (Fig. 2 D). However, in EB1-depleted cultures, CLIP-170 protein levels were unaffected (Fig. 2 C), but comet staining at MT plus ends was lost, whereas patches along the MT lattice remained detectable (Fig. 2 D). This was in line with the current model for EB1-mediated recruitment of CLIP-170 to MT plus ends. These observations, together with the effects of depleting either EB1 or CLIP-170 on HSV-1, suggested that plus end–associated, rather than lattice-bound CLIP-170, was important for early infection. To independently test this, the effect of dominant-negative EB1 was examined. Although C-terminal fluorescent tags do not interfere with EB1's ability to track growing MT plus ends, these large tags interfere with the recruitment of CLIP-170 through EB1's C terminus (Komarova et al., 2005; Lomakin et al., 2009; Skube et al., 2010). In line with these studies in other cell types, although dominant-negative EB1-mCherry (EB1-DN) formed

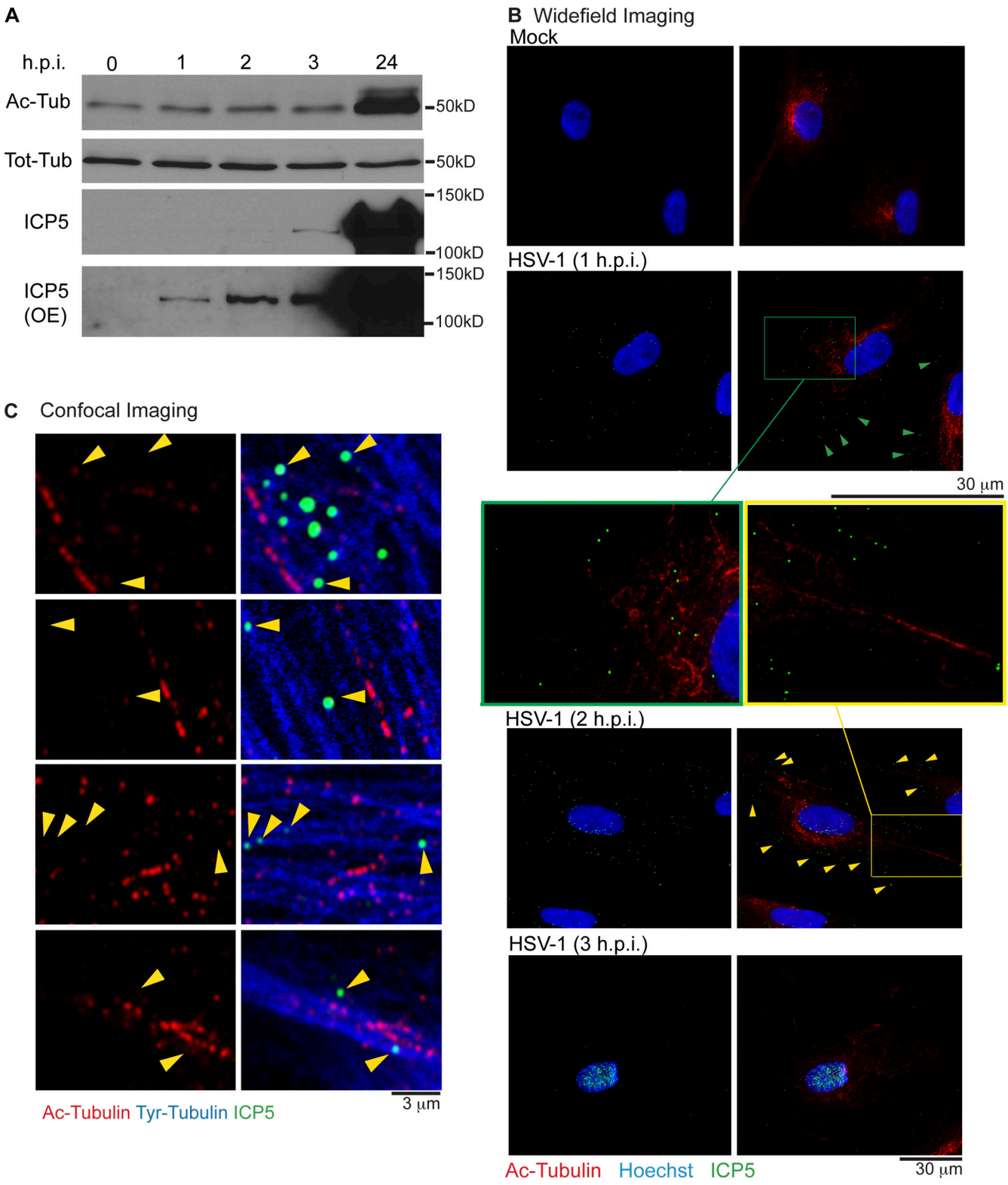

Figure 1. **HSV-1 capsids localize to dynamic MTs during early infection.** (A and B) NHDFs were mock infected (0 h) or infected with HSV-1 at MOI 20 for the indicated times in hpi. (A) Whole cell extracts were analyzed by immunoblotting with antibodies against the total or acetylated forms of tubulin. Detection of the major capsid protein ICP5, was used to illustrate infection of samples at each point, with overexposed (OE) blots showing the presence of viral capsids in samples as early as 1 hpi (B) Fixed samples were stained for Ac-tubulin (Ac-MTs; red) or capsid protein, ICP5 (green). Nuclei were stained using Hoechst. Samples were imaged by widefield microscopy. Green and yellow arrowheads point to representative capsids with no obvious localization to Ac-MTs. Magnified regions further illustrating this are highlighted by green and yellow boxes. (C) NHDFs were infected at MOI 20 for 1 h. Fixed samples were stained for ICP5 (green), Tyr-tubulin (blue), or Ac-tubulin (red). Representative confocal planes are shown. Arrowheads point to examples of capsids localized to Tyr-MTs with little or no marks of acetylation.

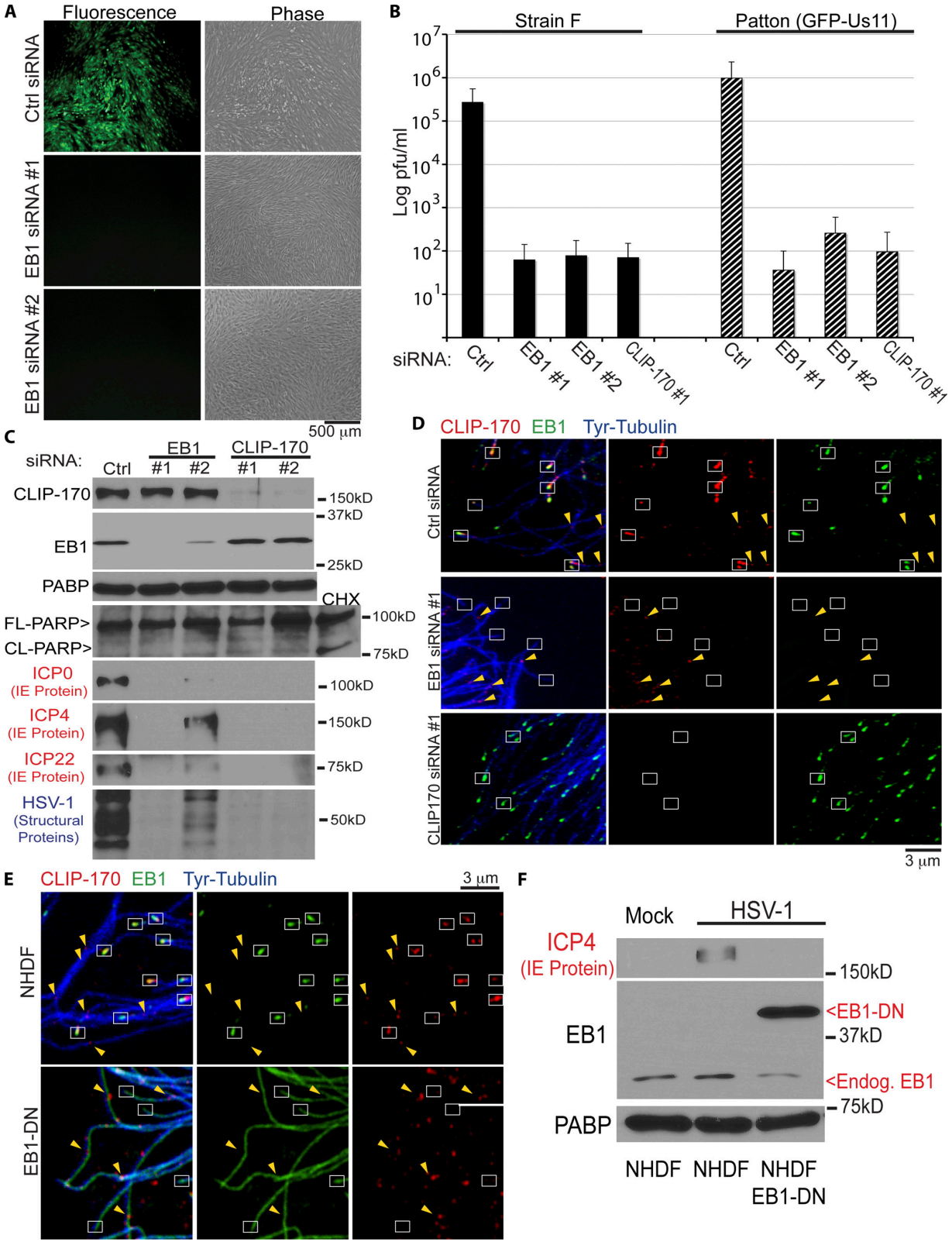

Figure 2. **EB1 and CLIP-170 are required for early HSV-1 infection.** (A) NHDFs were treated with control or independent EB1 siRNAs (#1 or #2) and then infected with HSV-1–GFP-Us11 at MOI 5 for 16 h. Representative fluorescence (GFP-Us11) and phase images are shown. (B) NHDFs were treated with control, EB1, or CLIP-170 siRNAs and then infected at MOI 5 for 16 h with either of two different HSV-1 strains: wild-type strain F or strain Patton (Patton (GFP-Us11)). Levels of infectious virus in freeze-thawed culture lysates are presented on a log scale of plaque forming units (pfu) per milliliter. Error bars represent standard deviation. (C) NHDFs were treated with control, EB1, or CLIP-170 siRNAs and then infected at MOI 5 for 16 h with HSV-1 (Patton (GFP-Us11)). Whole cell extracts were analyzed by WB with the indicated antibodies. ICP0, ICP4, and ICP22 are IE proteins, whereas anti–HSV-1 antibody detects several viral structural proteins made later in infection. A sample of control siRNA–treated NHDFs was treated with 100 μg/ml cycloheximide (CHX) for 4 h to induce the onset of apoptosis as a control for detection of PARP cleavage. (D) NHDFs were treated with control, EB1, or CLIP-170 siRNAs

tip-tracking comets in NHDFs (Video 1 A), IF analysis revealed that CLIP-170 was specifically displaced from MT plus ends in these cells (Fig. 2 E). Notably, similar to EB1 depletion above, patches of CLIP-170 along the MT lattice continued to be detected (Fig. 2 E). When NHDFs expressing EB1-DN were infected with HSV-1, expression of viral IE protein was potently suppressed compared with control NHDFs (Fig. 2 F). Notably, MT growth persists in EB1-DN–expressing NHDFs (Video 1 A), suggesting its effect on viral infection reflected the failure to recruit CLIP-170 rather than effects on dynamic MTs themselves. These independent approaches demonstrated that early HSV-1 infection was highly dependent on EB1 and CLIP-170 recruitment to dynamic MT plus ends.

To determine whether this block to infection represented effects on HSV-1 fusion and entry, siRNA-treated cultures were infected, fixed, and then stained for the capsid protein ICP5 (stained green) or the envelope glycoprotein gB (stained red). Viruses that have not fused stain for both proteins and appear yellow, glycoprotein that has been shed appears red, and particles that have entered the cytoplasm and lost their envelope appear green. Confocal microscopy and quantification of yellow versus green particles revealed no significant differences in the numbers and ratios of yellow and green particles in +TIP-depleted NHDFs compared with control samples (Fig. 3, A and B). As a positive control for this assay, all virus particles appeared yellow in NHDFs infected at 4°C to block fusion (Fig. 3, A and B). These findings were validated using a second entry assay (Jovasevic et al., 2008). In brief, cells were infected at 4°C to allow virus attachment and then returned to 37°C to allow entry. Unfused surface-bound virus was removed using citric acid buffer and proteinase K treatment, and then amounts of viral DNA in the cell were measured by quantitative real-time PCR (qRT-PCR). In line with IF-based fusion assays, results showed that the levels of viral DNA detected in cells was unaffected by depletion of either EB1 or CLIP-170 compared with control samples (Fig. 3 C). Infected samples maintained at 4°C demonstrated efficient removal of unpenetrated virus (Fig. 3 C). Depletion of EB1 and CLIP-170 in this experimental setup was confirmed by WB (Fig. 3 D). Overall, these findings demonstrated that EB1 and CLIP-170 did not affect viral fusion and entry into the cytosol. Moreover, the fact that the potent block to infection and IE protein production persisted at 16 hpi revealed that these +TIPs functioned in an early post-entry process critical to establishing infection.

HSV-1 requires CLIP-170 and its binding partners, EB1 and DCTN1, to initiate retrograde transport

Although virus particles entered the cytosol in +TIP-depleted cells, to determine whether their translocation to the nucleus was affected, NHDFs were treated with control, EB1, or CLIP-170 siRNAs and then infected with HSV-1 for 4 h. WB analysis confirmed target depletion by siRNAs in each case (Fig. 3 E), whereas fixed samples were stained for viral capsid protein, ICP5, and Tyr-tubulin. IF analysis revealed that in control cultures capsids accumulated at the nucleus (Fig. 3 F). A notable change in MT organization was also observed with clear loss of centrosomal focus of Tyr-MTs similar to previous studies (Avitabile et al., 1995; Naghavi et al., 2013; Pasdeloup et al., 2013). In contrast, in cells depleted of either EB1 or CLIP-170, capsids remained scattered and distant from the nucleus (Fig. 3 F). Furthermore, Tyr-MTs maintained centrosomal focus similar to uninfected cells, with no detectable loss of overall Tyr-MT mass or organization (Fig. 3 F). This established that depletion of EB1 or CLIP-170 did not block infection by causing gross defects in MT organization in NHDFs and suggested direct functions for EB1 and CLIP-170 in the transport of viral particles by dynamic MT filaments.

To verify that MT-based movement was indeed important for HSV-1 infection in these cells, NHDFs were treated with DMSO solvent control or the dynein inhibitor ciliobrevin D (Firestone et al., 2012). Cultures were then infected for 3 h before fixing and staining for Tyr-tubulin and capsid protein, ICP5. Fixed imaging revealed that, compared with DMSO controls, ciliobrevin D prevented virus particles from reaching the nucleus, and this occurred without effects on overall Tyr-MT organization (Fig. 4 A). Moreover, live cell imaging of HSV-1 containing a GFP-tagged capsid protein (K26GFP; Desai and Person, 1998) demonstrated that virus particles exhibited "twitchy" short-range motility as well as short bursts of longer-range transport, yet failed to reach the nucleus (Video 1 B). This was in stark contrast to the motility of virus particles in untreated NHDFs, shown and discussed in more detail later. To determine whether EB1 or CLIP-170 depletion altered dynein distribution, which might explain their effects on infection, siRNA-treated NHDFs were fixed and stained for dynein intermediate chain (DIC) and Tyr-tubulin. Imaging revealed no gross differences in the general distribution of DIC in NHDFs depleted of EB1 or CLIP-170 compared with control cultures (Fig. 4 B). DIC accumulation at the centrosome was also unaffected, in line with observations above that neither EB1 nor CLIP-170 affected overall Tyr-MT mass or anchoring. Similar results were observed for the large subunit of the dynein-activating complex, dynactin-1 (DCTN1/p150Glued; Fig. S2; Kardon and Vale, 2009; Vallee et al., 2012). However, DIC and DCNT1 staining patterns appeared more diffuse in peripheral regions of EB1- or CLIP-170–depleted cells when compared with the flecked patterns more readily observed in control samples. This was in line with previous studies that EB1 and CLIP-170 locally recruit DCTN1 to MT plus ends (Vaughan et al., 1999; Komarova et al., 2002, 2005; Goodson et al., 2003; Lansbergen et al., 2004; Watson and Stephens, 2006; Bjelić et al., 2012). Testing HSV-1's relative requirement for these proteins, the accumulation of viral IE and structural proteins was found to be potently suppressed in NHDFs treated with EB1, CLIP-170, or either of two independent DCTN1 siRNAs (Fig. 4 C).

and then fixed and stained for Tyr-tubulin (blue), EB1 (green), or CLIP-170 (red). Representative confocal planes are shown. White boxes highlight MT end staining with EB1, or MT ends lacking EB1 or CLIP-170 in EB1-depleted cells. Yellow arrowheads highlight examples of CLIP-170 patches localized along the MT lattice. (E) NHDFs or NHDFs expressing dominant-negative EB1 (EB1-DN) were fixed and stained for Tyr-tubulin (blue), EB1 (green), or CLIP-170 (red). Representative confocal planes are shown. White boxes highlight MT ends with EB1 and CLIP-170 in NHDFs, or MT ends lacking CLIP-170 in EB1-DN cells. Yellow arrowheads highlight examples of CLIP-170 patches localized along the MT lattice under each condition. Exposure settings required to image endogenous EB1 saturate images in EB1-DN–expressing cells, which also accumulates at MT plus ends (Video 1 A). (F) NHDF or NHDF-EB1-DN were mock infected or infected at MOI 5 for 5 h and then whole cell lysates were analyzed by WB using the indicated antibodies. Migration of endogenous EB1 and EB1-DN are highlighted to the right. FL, full length, CL, cleaved forms of PARP.

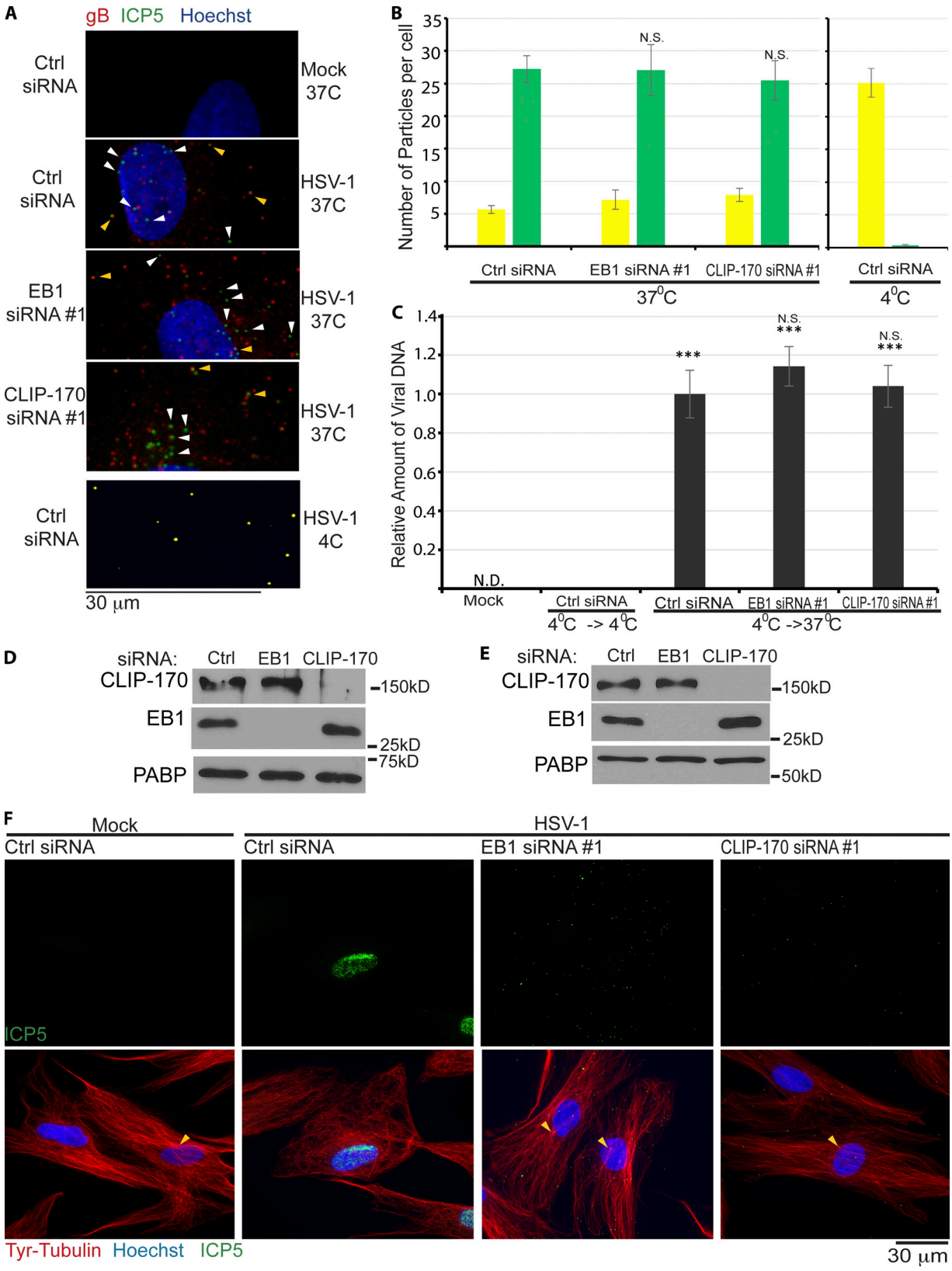

Figure 3. **EB1 and CLIP-170 mediate early post-entry infection.** (A) NHDFs were treated with control, EB1, or CLIP-170 siRNAs and infected at MOI 30 for 1 h. Samples were stained for viral glycoprotein, gB (red), or capsid protein, ICP5 (green). Nuclei were stained with Hoechst (blue). Particles lacking envelope (green) or with envelope (yellow) are indicated with white or yellow arrowheads, respectively. 4°C controls illustrate detection of unfused virus particles (yellow). Images were acquired by confocal microscopy, and representative planes are shown. (B) Random fields of view from samples in A were used to quantify unfused (yellow) and fused (green) particles. (Side) Control samples infected at 4°C. n = 18 cells with 18–45 particles per cell. Error bars represent standard error of the mean. Statistical analysis demonstrated no significant differences between control and EB1 or CLIP-170 siRNA–treated sam-

Moreover, DCTN1 depletion was also found to block the accumulation of viral particles at the nucleus when compared with control samples (Fig. 4 D), similar to the effects of EB1 or CLIP-170 depletion observed earlier (Fig. 3 F). This pointed to a potentially critical role in early HSV-1 infection for CLIP-170's proposed function in DCTN1 recruitment and cargo capture by dynamic MT plus ends (Vaughan et al., 1999; Watson and Stephens, 2006; Mishima et al., 2007; Slep and Vale, 2007; Bieling et al., 2008; Moughamian et al., 2013).

However, as outlined in more detail in the Discussion, there is considerable debate about the nature of cargoes captured through CLIP-170 for transport, which appear in most cases to be limited to a very small number of highly specialized cargoes or restricted to specific cell types. As studies to date have used transformed cell lines or nonhuman cells, one possibility was that this capture process is widely used in primary human fibroblasts. To test this, potential effects on early endosomes were first examined. NHDFs were treated with EB1 or CLIP-170 siRNAs, and fixed samples were stained for the early endosome marker, EEA1, and Tyr-tubulin. Imaging revealed no detectable differences in the overall distribution of EEA1-positive endosomes in cells depleted of either CLIP-170 or EB1 compared with control siRNA–treated cultures (Fig. 5 A). Quantification of early endosome fluorescence intensity or mean distances from the nucleus also revealed no significant differences between +TIP-depleted and control cultures (Fig. 5 B). To test this further, endocytic uptake of fluorescently labeled transferrin was examined. Imaging of the distribution of transferrin-positive vesicles and the fluorescence intensity of samples revealed that the uptake and localization of transferrin was unaffected by either EB1, CLIP-170, or DCTN1 depletion compared with control cultures (Fig. 5, C and D). In contrast, inhibition of dynein using ciliobrevin D reduced transferrin uptake and blocked the perinuclear accumulation of transferrin in NHDFs compared with DMSO-treated controls (Fig. S3, A and B). Next, potential effects on dynein-mediated transport of mitochondria or acidified vesicles (endosomes/lysosomes) were examined. When siRNA-treated NHDFs were stained with MitoTracker or LysoTracker, live cell imaging revealed no gross differences in the overall distribution or motility of either cargo in +TIP-depleted NHDFs: mitochondria remained filamentous in shape and continued to move rapidly throughout the cell (Fig. 5 E, Video 2, and Video 3), and lysosomes continued to accumulate and exhibit crowded movements around the nucleus while exhibiting long bidirectional runs in less densely occupied areas of the cytoplasm (Fig. 5 E, Video 4, and Video 5). Indeed, continued perinuclear accumulation of these cargoes in +TIP-depleted cells indicated no gross defects in their dynein-mediated transport, in line with previous observations in other cell types (Watson and Stephens, 2006). In stark contrast, dynein inhibition using ciliobrevin D caused gross changes in both cargoes: lysosomes no longer accumulated around the nucleus and exhibited short-range movements at the cell periphery (Fig. 5 F and Video 6), whereas mitochondria lost their filamentous form and dispersed to the cell periphery (Fig. 5 F and Video 7). Although more subtle effects on movement cannot be ruled out, these findings demonstrated that dynein-mediated transport and subcellular localization of these host cargoes had little or no requirement for EB1, CLIP-170, or DCTN1 in primary human fibroblasts.

The effects of +TIP depletion thus far suggested that HSV-1 particles were particularly reliant on CLIP-170–mediated capture for their transport. In line with this, virus particles, detected using anti-ICP5 antibody, could be observed colocalizing with CLIP-170 and Tyr-MT filaments in IF images of infected NHDFs (Fig. 6 A). Quantification revealed that ∼16% of virus particles colocalized with CLIP-170 in these samples (Fig. S4 A), as might be expected for a transient, dynamic capture process. Moreover, colocalization between virus particles and CLIP-170 could not be detected in samples depleted of EB1 (Fig. S4 B). To explore this further, HSV-1 localization and movement was examined using virus containing a GFP-tagged capsid protein (K26GFP; Desai and Person, 1998). In this case, virus particles stained with anti-GFP antibody could be observed colocalizing with both EB1 and CLIP-170 on Tyr-MTs (Fig. 6 B). Although this provided additional evidence that HSV-1 might serve as a target for CLIP-170–mediated capture, to functionally test this, the effects of +TIP depletion on virus transport were examined. Earlier IF analysis demonstrated that many nuclei became heavily decorated by viral capsids at 3 hpi (Fig. 1 B). As such, siRNA-treated NHDFs were infected with K26GFP for 3 h to ensure virus particles initiated transport in control samples and to determine the potential effects of +TIP depletion on their movement. Virus particles were then imaged at 1 frame per second (fps), with intermittent capture of Hoechst-stained nuclei. Under these conditions, virus particles were observed at different stages of movement to the nucleus in control siRNA–treated NHDFs. In most cases, nuclei were brightly lit with many locally moving virus particles, reflecting those that had docked and remain on nuclear pores (Roizman et al., 2007). In other cases, virus particles could be seen approaching and docking at the nuclear periphery, exhibiting rapid movements typical of MT-based bidirectional motility (Fig. 6 C and Video 8). Viruses were also observed moving in and out of, and even forming, perinuclear clusters that represent accumulation at the centrosome en route to the nucleus (Video 8). In stark contrast, in NHDFs depleted of EB1, CLIP-170, or DCTN1, capsids failed to initiate long-range retrograde transport toward the nucleus and exhibited short-range movements at the cell periphery, characteristic of actin-based motility (Fig. 6 C, Video 9, and Video 10). In line with this, fixed imaging revealed that in contrast to control cultures where HSV-1 reached the nucleus,

ples (one-way ANOVA; n = 18/group; $F_{(2,51)}$ = 0.096; P = 0.909). (C) Virus entry assay. NHDFs were mock infected or infected at MOI 30 at 4°C. Cultures were either maintained at 4°C (4°C→4°C) as a control for unfused virus, or shifted to 37°C (4°C→37°C) to allow virus entry. After removal of unpenetrated virus, viral DNA levels in cell lysates were measured by qRT-PCR. Error bars represent standard error of the mean. ***, P < 0.0001 versus control group at 4°C (one-way ANOVA; n = 3/group; $F_{(3,8)}$ = 98.588; P < 0.0001). Post-hoc analysis revealed levels of viral DNA in infected cells were unaffected by depletion of either EB1 (P = 0.377) or CLIP-170 (P = 0.960). (D) WB analysis of samples from cells that underwent 4°C→37°C shifting as described in C, confirming siRNA target depletion in each case. (E and F) NHDFs were treated with control, nontargeting siRNA, or siRNAs targeting either EB1 or CLIP-170. Cultures were then mock infected or infected at MOI 20 for 4 h. (E) WB analysis confirmed siRNA target depletion. (F) Fixed samples were stained for Tyr-tubulin (red) or the capsid protein ICP5 (green). Nuclei were stained with Hoechst (blue). Representative widefield images are shown. Arrowheads point to areas characteristic of centrosomal nucleation readily observed in either uninfected cells or infected cells depleted of EB1 or CLIP-170, but not detectable in control siRNA–treated cells infected with HSV-1. N.D., not detectable.

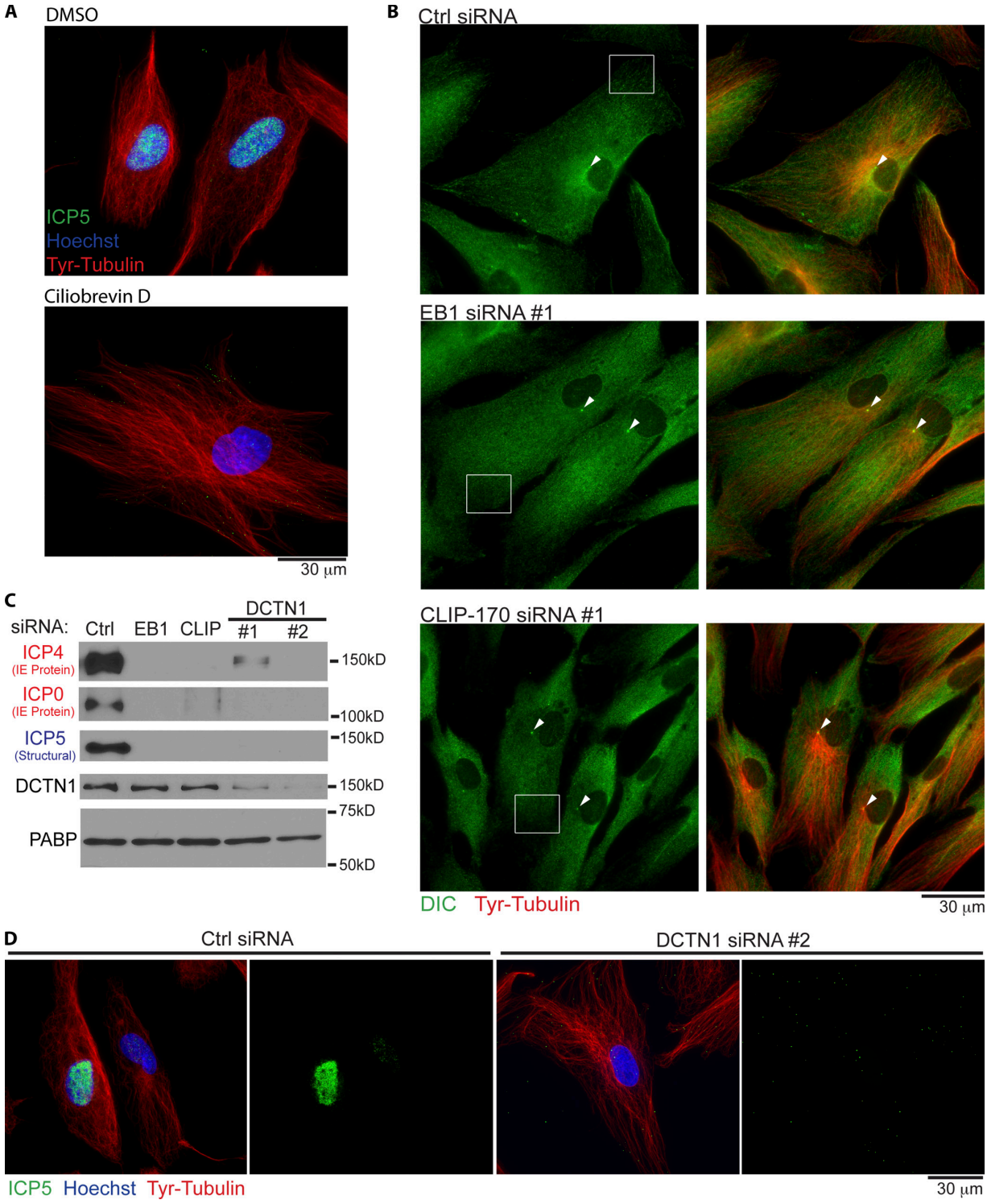

Figure 4. **Dynein and dynactin function in early HSV-1 infection of NHDFs.** (A) NHDFs were treated with DMSO solvent control or 200-µM ciliobrevin D for 1 h. Cultures were then infected with HSV-1 at MOI 30 for 3 h in the continued presence of inhibitor. Samples were then fixed and stained for Tyr-tubulin (red) or the major capsid protein ICP5 (green). Nuclei were stained with Hoechst. Representative widefield images are shown. (B) NHDFs were treated with control nontargeting, EB1, or CLIP-170 siRNAs and then fixed and stained for Tyr-tubulin (red) or DIC (green). Representative widefield images are shown. Arrowheads point to concentrations of DIC and Tyr-tubulin at centrosomes. Boxes highlight examples of flecked patterns of DIC staining at the cell periphery in control samples, which appear more diffuse in NHDFs depleted of either EB1 or CLIP-170. (C) NHDFs were treated with control, EB1, CLIP-170, or DCTN1 siRNAs and then infected with HSV-1 at MOI 5 for 6 h. Whole cell extracts were analyzed by WB with the indicated antibodies. Poly A–binding protein served as loading control. (D) NHDFs treated with control or DCNT1 siRNAs were infected with HSV-1 at MOI 20 for 4 h. Fixed samples were stained for Tyr-tubulin (red) or the capsid protein ICP5 (green). Nuclei were stained with Hoechst (blue). Representative widefield images are shown.

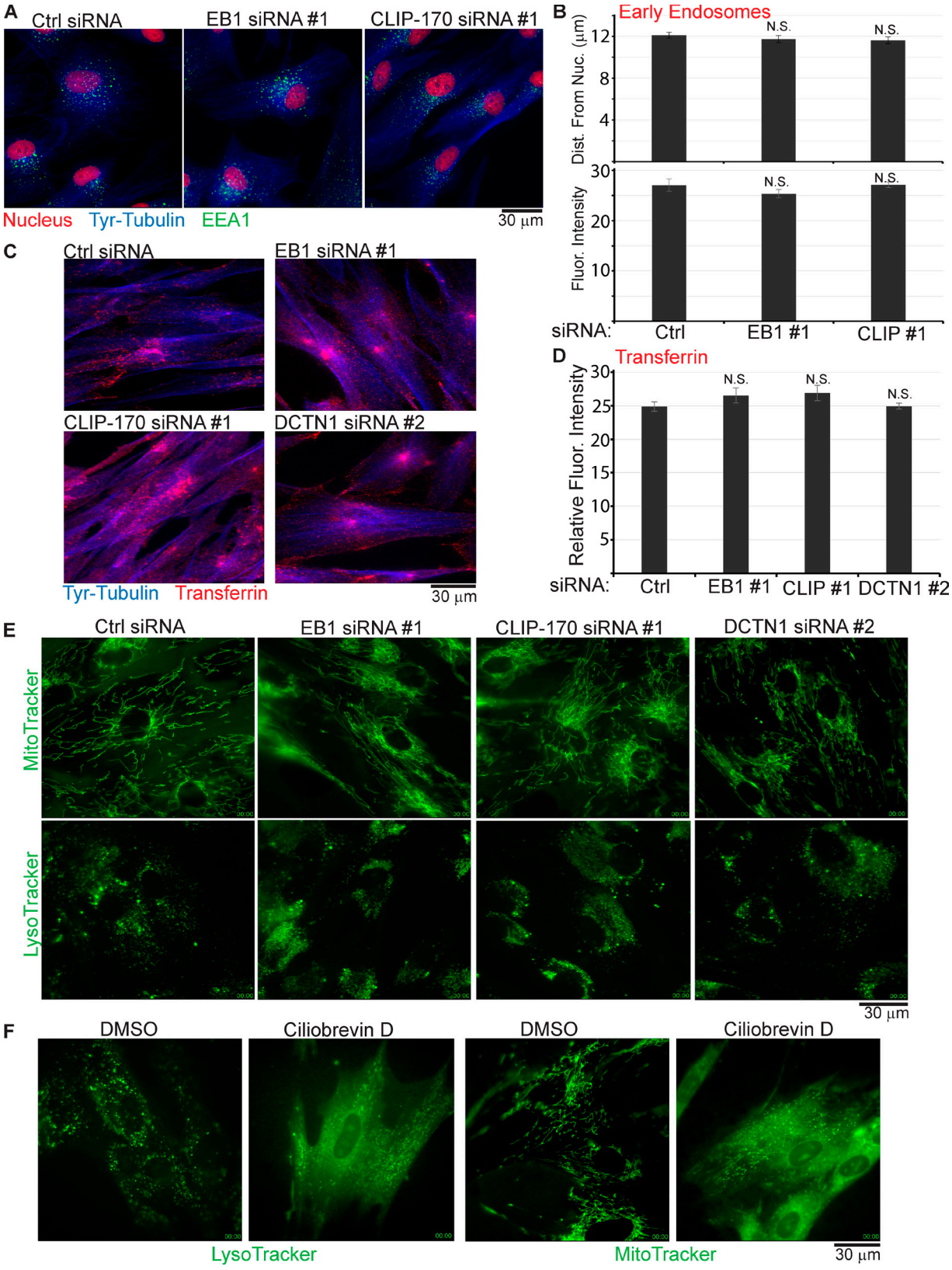

Figure 5. **Depletion of EB1, CLIP-170, or DCTN1 does not affect the distribution, uptake, or transport of various host cargoes.** (A–D) NHDFs were transfected with control (Ctrl), EB1, or CLIP-170 siRNAs. (A) Cultures were stained for the early endosomal marker, EEA1 (green), Tyr-tubulin (blue), or nuclei using DRAQ5 (red). Representative widefield images are shown. (B) Quantification of mean distance of endosomes from the nucleus per cell in each sample (top) and fluorescence intensity of endosome staining (bottom; arbitrary units) demonstrated no significant differences between control and EB1 or CLIP-170 siRNA-treated samples (one-way ANOVA; distance: n = 1,380/group; $F_{(4137,2)}$ = 0.281; P = 0.755; fluorescence intensity: n = 14/group; $F_{(39,2)}$ = 1.187; P = 0.316). (C) Cultures were incubated for 30 min with fluorescently labeled transferrin (red). Processed samples were then stained for

virus particles localized to phalloidin-stained actin filaments in NHDFs depleted of EB1, CLIP-170, or DCTN1 (Fig. S5). To independently validate these RNAi-based observations, NHDFs expressing EB1-DN that displaces CLIP-170 (Fig. 2 E) were infected and imaged in the same manner. Similar to +TIP-depleted NHDFs, expression of EB1-DN potently blocked long-range virus movement (Fig. 6 C and Video 10). These effects on virus motility were also noticeably different from the effects of dynein inhibition (Video 1 B), suggesting that these +TIPs functioned together and distinctly from dynein, as discussed below. Overall, these findings established that although several major host cargoes were not reliant on these +TIPs for their uptake, subcellular distribution, or movement in primary normal human fibroblasts, HSV-1 particles were exquisitely dependent on this capture mechanism involving EB1, CLIP-170, and DCTN1 to engage the host MT network and initiate retrograde transport.

Discussion

Findings reported here illustrating the role of CLIP-170 in early HSV-1 infection have important implications for our understanding of several biological processes. This includes the contribution of +TIPs to infection and insights into how viruses engage the host MT system, as well as fundamental mechanisms of selective cargo transport.

Although the importance of MTs to virus infection is well established (Radtke et al., 2006; Dodding and Way, 2011), in many cases the nature of the filaments involved (stable vs. dynamic) and their regulation remain poorly understood. Several viruses stimulate MT dynamics through upstream signal pathways, and this correlates with enhanced infection, but potential downstream effector +TIPs remain unknown (Suomalainen et al., 2001; Mabit et al., 2002; Arakawa et al., 2007; Roohvand et al., 2009). Conversely, Kaposi's sarcoma-associated herpesvirus, a γ-herpesvirus, stimulates Rho–Dia signaling to stabilize MTs during early infection (Naranatt et al., 2005). Recently, human immunodeficiency virus type 1 (HIV-1) was also found to rapidly stabilize MTs, and this study provided the first evidence of the functional importance of +TIPs EB1 and Kif4 to infection (Sabo et al., 2013). HSV-1 also induces MT stabilization, but to date this has only been examined at later stages of infection (Elliott and O'Hare, 1998; Naghavi et al., 2013). Again, recent work has uncovered functional roles for +TIPs in these events, with HSV-1 stabilizing MTs nucleated from the trans-Golgi network through the action of cytoplasmic linker–associated proteins to promote virus spread (Naghavi et al., 2013). Here, we demonstrate that HSV-1 does not induce MT stabilization at early time points and instead provide strong evidence for the functional importance of dynamic MT subsets in the early stages of infection. Moreover, we identify two different +TIPs, CLIP-170 and EB1, which associate with the growing ends of dynamic MTs, as playing a critical role in these events. As such, HSV-1 represents an elegant example of the extent to which viruses can exploit distinct MT subsets and their regulatory +TIPs to facilitate different stages of their life cycle.

Beyond adding to our understanding of the specific nature of MT subsets and +TIPs involved in infection, our findings also provide the first insights into how viruses actually engage host MTs to initiate transport. HSV-1 is known to interact with both dynein and kinesins and exhibits bidirectional movement in many cell types (Döhner et al., 2002, 2006; Douglas et al., 2004; Smith et al., 2004; Lee et al., 2006; Wolfstein et al., 2006; Apcarian et al., 2010; Radtke et al., 2010; McElwee et al., 2013; Zaichick et al., 2013). Notably, HSV-1 also interacts with dynactin, and dynactin perturbation through dynamitin overexpression results in a postinternalization block to HSV-1 accumulation at the nucleus (Döhner et al., 2002, 2006; Radtke et al., 2010). This was logically assumed to reflect dynactin's role as a dynein adaptor and stimulator of dynein motor activity (Kardon and Vale, 2009; Vallee et al., 2012; McKenney et al., 2014; Tripathy et al., 2014), which might serve as a means for HSV-1 to engage MTs. However, fixed imaging approaches used in prior studies did not determine the effects of dynamitin expression on virus transport. It is important to note that HSV-1 interacts directly with dynein intermediate and light chains, as well as interacting directly with dynactin independently of dynein (Ye et al., 2000; Döhner et al., 2002; Douglas et al., 2004; Wolfstein et al., 2006; Apcarian et al., 2010; Radtke et al., 2010; Zaichick et al., 2013). As such, the precise function of dynactin binding by HSV-1 particles has remained unclear. Our findings demonstrate that depletion of DCTN1 results in a potent block to HSV-1 transport, phenocopying the effects of removing the dynactin-recruiting complex of EB1 and CLIP-170 from MT plus ends using distinct approaches. Moreover, these effects on virus transport were quite distinct from the effects of dynein inhibition, wherein virus particles frequently made brief, erratic, and seemingly abortive longer-range movements, likely driven by association of particles with both kinesin and dynein. If dynactin simply functioned to stimulate dynein-mediated transport of HSV-1, reduced DCTN1 expression in siRNA-treated cells would be expected to result in similar motility to that observed in ciliobrevin D–treated NHDFs. This demonstrates that DCTN1 functions, at least in part, before dynein-mediated transport of HSV-1. As such, our findings shed new light on some of the very earliest stages of virus infection. Analogous to how viruses exploit specific surface molecules to engage and enter target cells, CLIP-170 on MT plus ends could be seen as a receptor required by dynactin-bound HSV-1 to engage MTs after entry. Another fundamental implication of these observations is that virus particles that enter the cytosol are not free to randomly associate with MT filaments but, instead, rely heavily upon this specialized capture process.

These observations also have important implications for our broader understanding of selective transport mechanisms in normal human cells. Indeed, there is considerable debate and disagreement over the nature of cargoes captured by CLIP-170. This process involves two key domains in CLIP-170; its

Tyr-tubulin (blue) and imaged. Representative widefield images are shown. (D) Transferrin uptake was determined by quantifying the fluorescence intensity of transferrin signal (arbitrary units) in samples described in C. No statistical difference was observed (one-way ANOVA; $n = 20$/group; $F_{(76,2)} = 1.347$; $P = 0.265$). (E) NHDFs were treated with control, EB1, CLIP-170, or DCTN1 siRNAs and then stained using MitoTracker or LysoTracker. Representative stills show mitochondria from Videos 2 and 3, or lysosomes from Videos 4 and 5. (F) NHDFs were treated with DMSO solvent control or 200-µM ciliobrevin D for 1 h and then stained using LysoTracker or MitoTracker. Representative still images show lysosomes from Video 6 or mitochondria from Video 7. Error bars represent standard error of the mean.

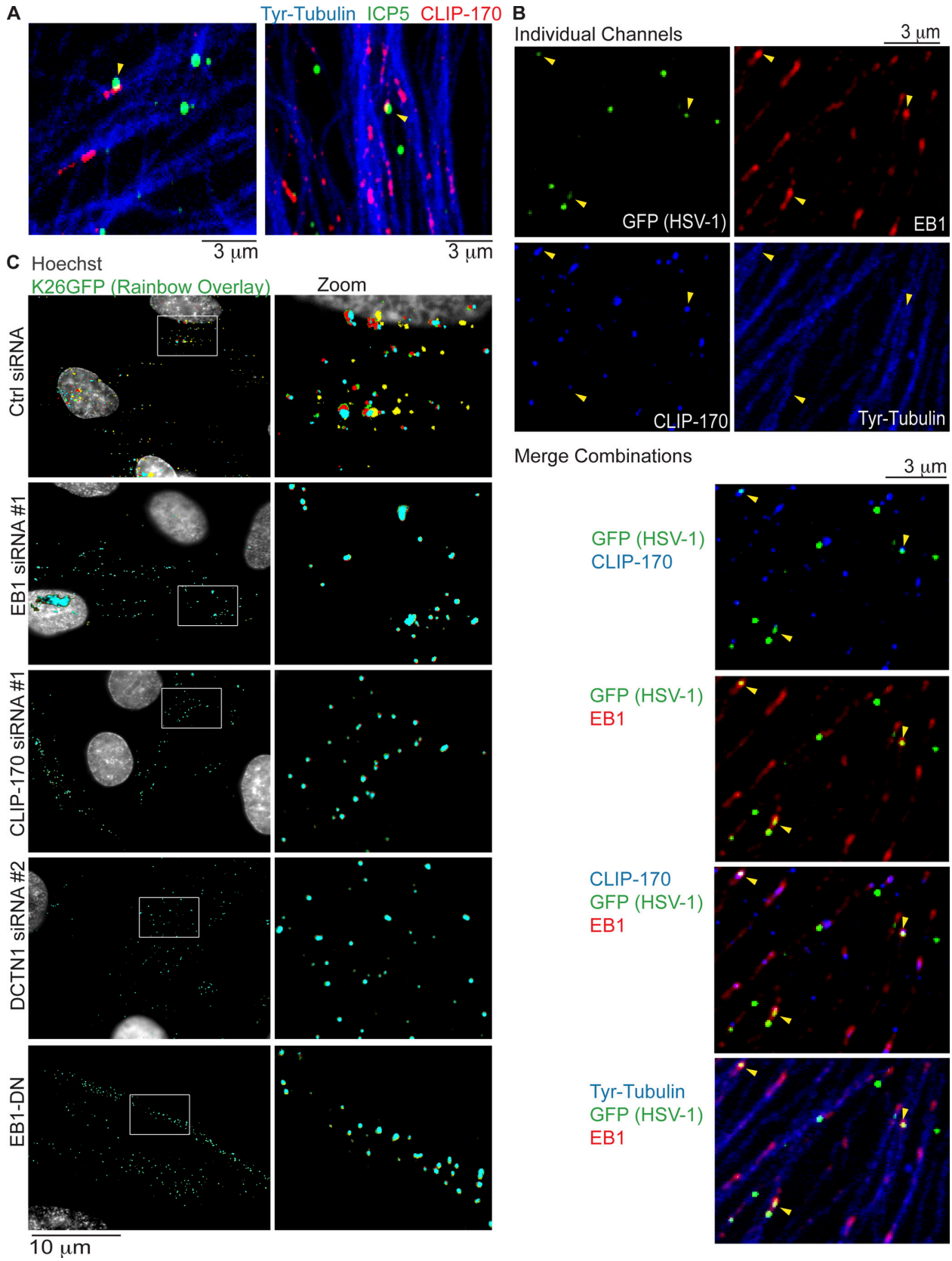

Figure 6. **Retrograde transport of HSV-1 requires EB1, CLIP-170, and DCTN1.** (A and B) NHDFs were infected with wild-type HSV-1 or HSV-1 K26GFP at MOI 60 for 30 min. (A) Wild type–infected samples were stained for the major capsid protein ICP5 (green), CLIP-170 (red), or Tyr-tubulin (blue). Representative confocal images are shown. Arrowheads point to examples of virus particles colocalizing with CLIP-170. (B) K26GFP-infected samples were stained for GFP (green), EB1 (far red), CLIP-170 (red; false-colored blue for merges), or Tyr-tubulin (blue). Representative confocal images are shown, and merge combinations are provided beneath. Arrowheads point to examples of virus particles colocalizing with EB1 and/or CLIP-170. (C) NHDFs were treated

N-terminal CAP-Gly motifs bind EB1, while its C-terminal zinc knuckle motifs bind dynactin (Pierre et al., 1992; Valetti et al., 1999; Goodson et al., 2003; Lansbergen et al., 2004; Watson and Stephens, 2006; Hayashi et al., 2007; Weisbrich et al., 2007; Gupta et al., 2009; Lee et al., 2010; Moughamian et al., 2013). Although CLIP-170 can bind tubulin and was the first +TIP discovered (Perez et al., 1999), its specific accumulation and function at MT plus ends in numerous mammalian cell lines requires EB1 (Vaughan et al., 1999, 2002; Lansbergen et al., 2004; Komarova et al., 2005; Ligon et al., 2006; Watson and Stephens, 2006; Mishima et al., 2007; Slep and Vale, 2007; Bieling et al., 2008; Moughamian et al., 2013). Our findings support this as a recruitment mechanism that also operates in primary normal human fibroblasts. Although CLIP-170 functions in linking MTs to different targets (Galjart, 2005), clues to its potential role in capturing cargoes destined for transport came from studies showing that CLIP-170 associated with endocytic vesicles (Rickard and Kreis, 1990) and colocalized with dynactin at MT tips (Vaughan et al., 1999). Early studies implicated CLIP-170 together with DCTN1 in kinetochore capture (Dujardin et al., 1998; Tai et al., 2002) as well as early endosome transport (Pierre et al., 1992; Valetti et al., 1999). However, functional aspects of these latter studies were based on effects of dynamitin overexpression, and several more recent studies have reported no effects of EB1, CLIP-170, or DCTN1 depletion, or deletion of the dynactin CAP-Gly domain that interacts with CLIP-170 or EB1, on the transport or distribution of endosomes/lysosomes (Goodson et al., 2003; Lansbergen et al., 2004; Watson and Stephens, 2006; Kim et al., 2007; Dixit et al., 2008). CLIP-170 is also dispensable for endosome transport in fungi (Lenz et al., 2006), although mechanisms of CLIP-170 regulation and recruitment differ significantly in lower organisms compared with mammals (Galjart, 2005). CLIP-170 also affects the surface organization of E-cadherin but does so without affecting E-cadherin transport or levels at the plasma membrane (Stehbens et al., 2006). Moreover, depletion of CLIP-170 or EB1 specifically removes DCTN1 from MT tips but does not affect broader organelle distribution, ER to Golgi transport, endosome and lysosome motility, or transferrin uptake in many cell types (Goodson et al., 2003; Lansbergen et al., 2004; Watson and Stephens, 2006; Kim et al., 2007; Dixit et al., 2008), and here we report similar observations in primary normal human cells.

Recently, however, it has been suggested that CLIP-170 may only be required for high-flux capture events or the capture of specialized cargoes. In line with this latter suggestion, the transport of EGF receptor–containing endosomes requires CLIP-170, but only when cells are stimulated with EGF (Hanafusa et al., 2011; Kedashiro et al., 2015). In *Xenopus laevis* melanosomes, CLIP-170 mediates the capture and transport of membrane-bounded pigment granules, or melanophores, although in this case it does not involve dynactin and the bridging factor remains unknown (Lomakin et al., 2009). Supporting a high-flux concept, the transport of several cargoes is initiated by EB1 and CLIP-170 at the distal ends of axons from mice, yet neither factor is required for transport in the mid-axon (Moughamian and Holzbaur, 2012; Moughamian et al., 2013). This broader role in cargo transport is not reported in other cell types, potentially reflecting specialized functions for CLIP-170 in neurons. Whether this is also observed in human neurons would be of interest given the significant differences in CLIP-170 function between species (Galjart, 2005). Our findings identify HSV-1 particles as novel, nonhost cargoes that exploit CLIP-170–mediated capture under conditions where this process is dispensable to many host cargoes in primary normal human cells, including transferrin uptake that might be expected to involve high flux and that reflects another cargo taken into the cell. As such, these virus particles join melanophores and EGF receptor–containing endosomes as one of the few specialized cargoes that are highly dependent on capture by CLIP-170, outside of neuronal cells. Although CLIP-170 knockout mice exhibit defects in spermatogenesis, they are viable and appear otherwise normal (Akhmanova et al., 2005), suggesting that specific +TIPs, such as CLIP-170, that are required for infection could serve as potential targets in the development of potent new antivirals.

Materials and methods

Cells, viruses, and chemicals

NHDFs and Vero cells were cultured in DMEM containing 5% FBS, 1% L-glutamine, and 1% penicillin-streptomycin (Walsh and Mohr, 2004; Naghavi et al., 2013). HSV-1 strain F, HSV-1–GFP-Us11 (gifts from I. Mohr, New York University, School of Medicine, New York, NY), and HSV-1 K26GFP (a gift from P. Desai, Johns Hopkins University, Baltimore, MD) were propagated by infecting Vero cells in DMEM containing 1% FBS, 1% L-glutamine, and 1% penicillin-streptomycin (Desai and Person, 1998; Naghavi et al., 2013). Once 90–100% cytopathic effect was observed, infected cells were scraped into culture medium and lysed by three rounds of −80°C freezing and thawing. Cell debris was removed by centrifugation at 3,000 *g* for 4 min at 4°C. Stock titers were determined by serial dilution and infection of Vero cells, followed by plaque counting 3 d later. Levels of infectious virus in cultures of NHDFs were determined by freeze-thaw lysis of cells scraped into culture media followed by serial dilution and titration on permissive Vero cells (Walsh and Mohr, 2004). Ciliobrevin D was procured from EMD Millipore. Phalloidin CF647 was purchased from VWR International. MitoTracker green and LysoTracker green were purchased from Cell Signaling Technology.

siRNAs, plasmids, and transfections

siRNAs were acquired from Applied Biosystems: control (AM4635 and AM4637), EB1 (3891 and 136501), CLIP-170 (142517 and 12224), and DCTN1 (14262 and 14174). Cells were transfected with 150 pmol/ml siRNA using RNAiMax (Invitrogen). 72 h later, cultures were infected as described in the Results. To generate mCherry-tagged EB1, human EB1 was cloned into pN1-mCherry (Takara Bio Inc.) and then subcloned into the lentiviral vector, pLVX (Takara Bio Inc.; Sabo et al., 2013). Lentivirus was produced by cotransfection of 293T cells with pLVX-EB1-mCherry (a gift from J. Sabo, Columbia University, New York, NY), p8.91 (group-specific antigen polymerase), and p-VSV-G

with control, EB1, CLIP-170, or DCTN1 siRNAs, or NHDFs expressing EB1-DN were infected with K26GFP at MOI 100 for 3 h. Nuclei were stained using Hoechst, and live cell microscopy was performed capturing images at 1 fps. Rainbow overlays, illustrating particle motility under each condition, were generated using representative frames from Videos 8, 9, and 10, as described in Materials and methods section Antibodies, WB, IF, and imaging. Nuclei were false-colored gray. Magnified images of boxed regions are presented to the right.

(envelope). Filtered supernatant containing lentivirus was then used to transduce NHDFs, and cultures were selected with hygromycin to generate pools of NHDFs stably expressing EB1-mCherry, which were then routinely maintained and cultured as described for NHDFs.

Antibodies, WB, IF, and imaging

Antibodies used in this study were as follows: EB1 (sc-47704) and CLIP-170 (sc-25613) from Santa Cruz Biotechnology, Inc.; PARP (9542), EEA1 (3288), Ac-tubulin (5335), and GFP (2965) from Cell Signaling Technology; DIC (MAB1618) from EMD Millipore; ICP0 (Ab6513), ICP4 (Ab6514), HSV-1 (Ab200535), and dynactin (Ab11806) from Abcam; and ICP5 (HA018) from Virusys. Anti-poly A–binding protein antibody was a gift from S. Morley (University of Sussex, Sussex, England, UK). Anti–Tyr-tubulin antibody was a gift from G. Gundersen (Columbia University, New York, NY). Anti-ICP22 antibody was a gift from J. Blaho (City College of New York, New York, NY). Anti-gB antibody was a gift from Q. Fan and R. Longnecker (Northwestern University, Chicago, IL). For IF, cultures were rinsed in PBS and fixed in ice-cold methanol for 7 min or 4% paraformaldehyde for 20 min. Samples were then blocked in PBS containing 10% FBS/0.25% saponin and subsequently incubated at 4°C overnight with the appropriate primary antibody diluted in PBS containing 10% FBS/0.025% saponin. The next day, samples were washed in PBS containing 0.025% saponin and then incubated with the appropriate Alexa Fluor–conjugated secondary antibody for 1 h at room temperature. After washing, samples were stained with Hoechst 33342 before washing and mounting in FluorSave reagent (EMD Millipore; Naghavi et al., 2013). Widefield images were acquired using a microscope (DMI6000B; Leica) with a 100× objective (HC PL APO 100×/1.44 NA oil), a camera (FLASH 4.0 cMOS; ORCA), and MetaMorph software (Molecular Devices). Confocal images were acquired using a motorized spinning-disk microscope (CSUX confocal head [Yokogawa]; DMI6000B microscope [Leica]), a 100× objective (HCX PL APO 100×/1.44 NA oil), a camera (X2 Back-Thinned EM charge-coupled device; ImagEM), and MetaMorph software. All analysis of fluorescence intensities, sizes, and distances were performed using MetaMorph analysis software. For live cell imaging, cells were seeded on 35-mm glass-bottom dishes (MatTek Corporation) and transfected or infected as described in the previous section and in the Results section. For imaging of viral particles and nuclei, after infection and immediately before imaging nuclei were stained with Hoechst 33342 and medium was changed to CO_2-independent medium (Gibco). Imaging was performed on a microscope (DMI6000B with adaptive focus control [AFC]; Leica) with an environmental chamber (InVivo) at 37°C using an oil objective (HC PL APO 100×/1.44 NA oil). Images were acquired at 1 fps over 6–7 min in the GFP channel, with intermittent capture of DNA staining through the DAPI channel, using a camera (FLASH 4.0 cMOS; ORCA) and MetaMorph software. Mitochondria were visualized by adding 100-nM MitoTracker 15 min before imaging at 0.3 fps. Lysosomes were visualized by adding 50-nM LysoTracker immediately before imaging at 2 fps. Within experiments, all samples were imaged using the same acquisition settings, and all postacquisition processing of contrast or intensity was minimized and applied equally throughout samples using MetaMorph or Photoshop (Adobe) software. To generate rainbow overlays, frames were extracted at equal intervals from videos, and GFP signal, representing virus particles, was assigned a different false color in each frame. Frames were then overlayed in Photoshop. Because of low-level drift (evident in corresponding videos), Hoechst-stained nuclei were used to accurately overlay each frame under each condition.

Viral entry and transferrin uptake assays

For viral entry assays, cells were incubated with HSV-1 at MOI 30 for 1 h at 4°C to allow virus binding. Experimental groups were then transferred to 37°C for 1 h, while a control group was maintained at 4°C. Cultures were then washed with PBS followed by washing with low-pH citrate buffer (40-mM sodium citrate, 10-mM KCl, and 135-mM NaCl, pH 3.0) to inactivate unpenetrated virus and then washed again with PBS. Cultures were then incubated with 2 mg/ml proteinase K (Invitrogen) at 37°C for 1 h to remove surface-attached, inactivated virus that had not entered cells. Cultures were then washed in PBS five times, collected by centrifugation (367 *g* for 5 min), and resuspended in PBS. DNA was isolated by phenol–chloroform extraction and dissolved in water. Viral DNA was detected by qRT-PCR using primers specific for HSV-1 DNA (forward, 5′-CCCACGGTCAGTCTGGTATC-3′; reverse, 5′-TTTGTGTCCCATGGGGTAGT-3′). The amount of viral DNA in siRNA-treated samples was expressed relative to control siRNA–treated cultures raised to 37°C and arbitrarily set to a value of 1 (Jovasevic et al., 2008). For transferrin uptake assays, medium on siRNA-treated NHDFs was replaced with serum-free medium containing Alexa Fluor 647–transferrin (Invitrogen) for 30 min at 37°C before being placed on ice and washed in low-pH citrate buffer. Cultures were then fixed in 4% paraformaldehyde and then stained with the indicated antibodies and imaged as described above.

Statistical analyses

Statistical analyses were performed using SPSS software (IBM). One-way analysis of variance (ANOVA) was followed by Scheffe's test for post-hoc comparisons of three or more experimental groups (only when ANOVA was significant). Homogeneity of variance was confirmed with Levene's test for equality of variances. The p-value for all cases was set to <0.05 for significant differences.

Online supplemental material

Fig. S1 shows grayscale images of Ac-MT staining from Fig. 1. Fig. S2 shows the effects of EB1 or CLIP-170 depletion on DCTN1 localization in NHDFs. Fig. S3 shows the effects of dynein inhibition, using ciliobrevin D, on transferrin uptake (A) and localization (B). Fig. S4 shows quantitation of the number of viral particles colocalized with CLIP-170 (A) and examples of viral particles that do not colocalize with lattice-associated CLIP-170 in EB1-depleted NHDFs (B). Fig. S5 shows the colocalization of viral particles with actin filaments in NHDFs depleted of EB1, CLIP-170, or DCTN1. Video 1 shows movement of EB1-DN (EB1-mCherry; false colored green for contrast) in NHDFs (A) and HSV-1 K26GFP in ciliobrevin D–treated NHDFs (B). Video 2 shows the movement of mitochondria in NHDFs treated with control siRNA or EB1 siRNA. Video 3 shows the movement of mitochondria in NHDFs treated with CLIP-170 siRNA or DCTN1 siRNA. Video 4 shows the movement of lysosomes in NHDFs treated with control siRNA or EB1 siRNA. Video 5 shows the movement of lysosomes in NHDFs treated with CLIP-170 siRNA or DCTN1 siRNA. Video 6 shows the movement of lysosomes in NHDFs treated with DMSO or ciliobrevin D. Video 7 shows the movement of mitochondria in NHDFs treated with DMSO or ciliobrevin D. Video 8 shows the movement of HSV-1 K26GFP in NHDFs treated with control siRNA. Video 9 shows the movement of HSV-1 K26GFP in NHDFs treated with EB1 siRNA or CLIP-170 siRNA. Video 10 shows the movement of HSV-1 K26GFP in NHDFs treated with DCTN1 siRNA or expressing EB1-DN. Online supplemental material is available at http://www.jcb.org/cgi/content/full/jcb.201505123/DC1.

Acknowledgments

We thank Greg Smith, Richard Longnecker, Qing Fan, Prashant Desai, Yosef Sabo, Ian Mohr, and John Blaho for reagents and support.

This work was supported by grants from the National Institutes of Health to M.H. Naghavi (R01GM101975 and P01GM105536) and D. Walsh (P01GM105536).

The authors declare no competing financial interests.

Submitted: 3 June 2015
Accepted: 17 September 2015

References

Akhmanova, A., A.L. Mausset-Bonnefont, W. van Cappellen, N. Keijzer, C.C. Hoogenraad, T. Stepanova, K. Drabek, J. van der Wees, M. Mommaas, J. Onderwater, et al. 2005. The microtubule plus-end-tracking protein CLIP-170 associates with the spermatid manchette and is essential for spermatogenesis. *Genes Dev.* 19:2501–2515. http://dx.doi.org/10.1101/gad.344505

Apcarian, A., A.L. Cunningham, and R.J. Diefenbach. 2010. Identification of binding domains in the herpes simplex virus type 1 small capsid protein pUL35 (VP26). *J. Gen. Virol.* 91:2659–2663. http://dx.doi.org/10.1099/vir.0.019984-0

Arakawa, Y., J.V. Cordeiro, and M. Way. 2007. F11L-mediated inhibition of RhoA-mDia signaling stimulates microtubule dynamics during vaccinia virus infection. *Cell Host Microbe.* 1:213–226. http://dx.doi.org/10.1016/j.chom.2007.04.007

Avitabile, E., S. Di Gaeta, M.R. Torrisi, P.L. Ward, B. Roizman, and G. Campadelli-Fiume. 1995. Redistribution of microtubules and Golgi apparatus in herpes simplex virus-infected cells and their role in viral exocytosis. *J. Virol.* 69:7472–7482.

Bieling, P., S. Kandels-Lewis, I.A. Telley, J. van Dijk, C. Janke, and T. Surrey. 2008. CLIP-170 tracks growing microtubule ends by dynamically recognizing composite EB1/tubulin-binding sites. *J. Cell Biol.* 183:1223–1233. http://dx.doi.org/10.1083/jcb.200809190

Bjelić, S., C.O. De Groot, M.A. Schärer, R. Jaussi, K. Bargsten, M. Salzmann, D. Frey, G. Capitani, R.A. Kammerer, and M.O. Steinmetz. 2012. Interaction of mammalian end binding proteins with CAP-Gly domains of CLIP-170 and p150^{glued}. *J. Struct. Biol.* 177:160–167. http://dx.doi.org/10.1016/j.jsb.2011.11.010

Desai, P., and S. Person. 1998. Incorporation of the green fluorescent protein into the herpes simplex virus type 1 capsid. *J. Virol.* 72:7563–7568.

Dixit, R., J.R. Levy, M. Tokito, L.A. Ligon, and E.L. Holzbaur. 2008. Regulation of dynactin through the differential expression of p150Glued isoforms. *J. Biol. Chem.* 283:33611–33619. http://dx.doi.org/10.1074/jbc.M804840200

Dodding, M.P., and M. Way. 2011. Coupling viruses to dynein and kinesin-1. *EMBO J.* 30:3527–3539. http://dx.doi.org/10.1038/emboj.2011.283

Döhner, K., A. Wolfstein, U. Prank, C. Echeverri, D. Dujardin, R. Vallee, and B. Sodeik. 2002. Function of dynein and dynactin in herpes simplex virus capsid transport. *Mol. Biol. Cell.* 13:2795–2809. http://dx.doi.org/10.1091/mbc.01-07-0348

Döhner, K., K. Radtke, S. Schmidt, and B. Sodeik. 2006. Eclipse phase of herpes simplex virus type 1 infection: Efficient dynein-mediated capsid transport without the small capsid protein VP26. *J. Virol.* 80:8211–8224. http://dx.doi.org/10.1128/JVI.02528-05

Douglas, M.W., R.J. Diefenbach, F.L. Homa, M. Miranda-Saksena, F.J. Rixon, V. Vittone, K. Byth, and A.L. Cunningham. 2004. Herpes simplex virus type 1 capsid protein VP26 interacts with dynein light chains RP3 and Tctex1 and plays a role in retrograde cellular transport. *J. Biol. Chem.* 279:28522–28530. http://dx.doi.org/10.1074/jbc.M311671200

Dujardin, D., U.I. Wacker, A. Moreau, T.A. Schroer, J.E. Rickard, and J.R. De Mey. 1998. Evidence for a role of CLIP-170 in the establishment of metaphase chromosome alignment. *J. Cell Biol.* 141:849–862. http://dx.doi.org/10.1083/jcb.141.4.849

Elliott, G., and P. O'Hare. 1998. Herpes simplex virus type 1 tegument protein VP22 induces the stabilization and hyperacetylation of microtubules. *J. Virol.* 72:6448–6455.

Firestone, A.J., J.S. Weinger, M. Maldonado, K. Barlan, L.D. Langston, M. O'Donnell, V.I. Gelfand, T.M. Kapoor, and J.K. Chen. 2012. Small-molecule inhibitors of the AAA+ ATPase motor cytoplasmic dynein. *Nature.* 484:125–129. http://dx.doi.org/10.1038/nature10936

Galjart, N. 2005. CLIPs and CLASPs and cellular dynamics. *Nat. Rev. Mol. Cell Biol.* 6:487–498. http://dx.doi.org/10.1038/nrm1664

Goodson, H.V., S.B. Skube, R. Stalder, C. Valetti, T.E. Kreis, E.E. Morrison, and T.A. Schroer. 2003. CLIP-170 interacts with dynactin complex and the APC-binding protein EB1 by different mechanisms. *Cell Motil. Cytoskeleton.* 55:156–173. http://dx.doi.org/10.1002/cm.10114

Gundersen, G.G. 2002. Evolutionary conservation of microtubule-capture mechanisms. *Nat. Rev. Mol. Cell Biol.* 3:296–304. http://dx.doi.org/10.1038/nrm777

Gupta, K.K., B.A. Paulson, E.S. Folker, B. Charlebois, A.J. Hunt, and H.V. Goodson. 2009. Minimal plus-end tracking unit of the cytoplasmic linker protein CLIP-170. *J. Biol. Chem.* 284:6735–6742. http://dx.doi.org/10.1074/jbc.M807675200

Hanafusa, H., K. Ishikawa, S. Kedashiro, T. Saigo, S. Iemura, T. Natsume, M. Komada, H. Shibuya, A. Nara, and K. Matsumoto. 2011. Leucine-rich repeat kinase LRRK1 regulates endosomal trafficking of the EGF receptor. *Nat. Commun.* 2:158. http://dx.doi.org/10.1038/ncomms1161

Hayashi, I., M.J. Plevin, and M. Ikura. 2007. CLIP170 autoinhibition mimics intermolecular interactions with p150^{Glued} or EB1. *Nat. Struct. Mol. Biol.* 14:980–981. http://dx.doi.org/10.1038/nsmb1299

Honnappa, S., S.M. Gouveia, A. Weisbrich, F.F. Damberger, N.S. Bhavesh, H. Jawhari, I. Grigoriev, F.J. van Rijssel, R.M. Buey, A. Lawera, et al. 2009. An EB1-binding motif acts as a microtubule tip localization signal. *Cell.* 138:366–376. http://dx.doi.org/10.1016/j.cell.2009.04.065

Jiang, K., and A. Akhmanova. 2011. Microtubule tip-interacting proteins: A view from both ends. *Curr. Opin. Cell Biol.* 23:94–101. http://dx.doi.org/10.1016/j.ceb.2010.08.008

Jovasevic, V., L. Liang, and B. Roizman. 2008. Proteolytic cleavage of VP1-2 is required for release of herpes simplex virus 1 DNA into the nucleus. *J. Virol.* 82:3311–3319. http://dx.doi.org/10.1128/JVI.01919-07

Kardon, J.R., and R.D. Vale. 2009. Regulators of the cytoplasmic dynein motor. *Nat. Rev. Mol. Cell Biol.* 10:854–865. http://dx.doi.org/10.1038/nrm2804

Kedashiro, S., S.I. Pastuhov, T. Nishioka, T. Watanabe, K. Kaibuchi, K. Matsumoto, and H. Hanafusa. 2015. LRRK1-phosphorylated CLIP-170 regulates EGFR trafficking by recruiting p150^{Glued} to microtubule plus ends. *J. Cell Sci.* 128:385–396. http://dx.doi.org/10.1242/jcs.161547

Kim, H., S.C. Ling, G.C. Rogers, C. Kural, P.R. Selvin, S.L. Rogers, and V.I. Gelfand. 2007. Microtubule binding by dynactin is required for microtubule organization but not cargo transport. *J. Cell Biol.* 176:641–651. http://dx.doi.org/10.1083/jcb.200608128

Komarova, Y., G. Lansbergen, N. Galjart, F. Grosveld, G.G. Borisy, and A. Akhmanova. 2005. EB1 and EB3 control CLIP dissociation from the ends of growing microtubules. *Mol. Biol. Cell.* 16:5334–5345. http://dx.doi.org/10.1091/mbc.E05-07-0614

Komarova, Y.A., A.S. Akhmanova, S. Kojima, N. Galjart, and G.G. Borisy. 2002. Cytoplasmic linker proteins promote microtubule rescue in vivo. *J. Cell Biol.* 159:589–599. http://dx.doi.org/10.1083/jcb.200208058

Kristensson, K., E. Lycke, M. Röyttä, B. Svennerholm, and A. Vahlne. 1986. Neuritic transport of herpes simplex virus in rat sensory neurons *in vitro*. Effects of substances interacting with microtubular function and axonal flow [nocodazole, taxol and erythro-9-3-(2-hydroxynonyl)adenine]. *J. Gen. Virol.* 67:2023–2028. http://dx.doi.org/10.1099/0022-1317-67-9-2023

Lansbergen, G., Y. Komarova, M. Modesti, C. Wyman, C.C. Hoogenraad, H.V. Goodson, R.P. Lemaitre, D.N. Drechsel, E. van Munster, T.W. Gadella Jr., et al. 2004. Conformational changes in CLIP-170 regulate its binding to microtubules and dynactin localization. *J. Cell Biol.* 166:1003–1014. http://dx.doi.org/10.1083/jcb.200402082

Lee, G.E., J.W. Murray, A.W. Wolkoff, and D.W. Wilson. 2006. Reconstitution of herpes simplex virus microtubule-dependent trafficking in vitro. *J. Virol.* 80:4264–4275. http://dx.doi.org/10.1128/JVI.80.9.4264-4275.2006

Lee, H.S., Y.A. Komarova, E.S. Nadezhdina, R. Anjum, J.G. Peloquin, J.M. Schober, O. Danciu, J. van Haren, N. Galjart, S.P. Gygi, et al. 2010. Phosphorylation controls autoinhibition of cytoplasmic linker protein-170. *Mol. Biol. Cell.* 21:2661–2673. http://dx.doi.org/10.1091/mbc.E09-12-1036

Lenz, J.H., I. Schuchardt, A. Straube, and G. Steinberg. 2006. A dynein loading zone for retrograde endosome motility at microtubule plus-ends. *EMBO J.* 25:2275–2286. http://dx.doi.org/10.1038/sj.emboj.7601119

Ligon, L.A., S.S. Shelly, M.K. Tokito, and E.L. Holzbaur. 2006. Microtubule binding proteins CLIP-170, EB1, and p150^{Glued} form distinct plus-end complexes. *FEBS Lett.* 580:1327–1332. http://dx.doi.org/10.1016/j.febslet.2006.01.050

Lomakin, A.J., I. Semenova, I. Zaliapin, P. Kraikivski, E. Nadezhdina, B.M. Slepchenko, A. Akhmanova, and V. Rodionov. 2009. CLIP-170-

dependent capture of membrane organelles by microtubules initiates minus-end directed transport. *Dev. Cell.* 17:323–333. http://dx.doi.org/10.1016/j.devcel.2009.07.010

Mabit, H., M.Y. Nakano, U. Prank, B. Saam, K. Döhner, B. Sodeik, and U.F. Greber. 2002. Intact microtubules support adenovirus and herpes simplex virus infections. *J. Virol.* 76:9962–9971. http://dx.doi.org/10.1128/JVI.76.19.9962-9971.2002

McElwee, M., F. Beilstein, M. Labetoulle, F.J. Rixon, and D. Pasdeloup. 2013. Dystonin/BPAG1 promotes plus-end-directed transport of herpes simplex virus 1 capsids on microtubules during entry. *J. Virol.* 87:11008–11018. http://dx.doi.org/10.1128/JVI.01633-13

McKenney, R.J., W. Huynh, M.E. Tanenbaum, G. Bhabha, and R.D. Vale. 2014. Activation of cytoplasmic dynein motility by dynactin-cargo adapter complexes. *Science.* 345:337–341. http://dx.doi.org/10.1126/science.1254198

Mishima, M., R. Maesaki, M. Kasa, T. Watanabe, M. Fukata, K. Kaibuchi, and T. Hakoshima. 2007. Structural basis for tubulin recognition by cytoplasmic linker protein 170 and its autoinhibition. *Proc. Natl. Acad. Sci. USA.* 104:10346–10351. http://dx.doi.org/10.1073/pnas.0703876104

Moughamian, A.J., and E.L. Holzbaur. 2012. Synaptic vesicle distribution by conveyor belt. *Cell.* 148:849–851. http://dx.doi.org/10.1016/j.cell.2012.02.007

Moughamian, A.J., G.E. Osborn, J.E. Lazarus, S. Maday, and E.L. Holzbaur. 2013. Ordered recruitment of dynactin to the microtubule plus-end is required for efficient initiation of retrograde axonal transport. *J. Neurosci.* 33:13190–13203. http://dx.doi.org/10.1523/JNEUROSCI.0935-13.2013

Naghavi, M.H., G.G. Gundersen, and D. Walsh. 2013. Plus-end tracking proteins, CLASPs, and a viral Akt mimic regulate herpesvirus-induced stable microtubule formation and virus spread. *Proc. Natl. Acad. Sci. USA.* 110:18268–18273. http://dx.doi.org/10.1073/pnas.1310760110

Naranatt, P.P., H.H. Krishnan, M.S. Smith, and B. Chandran. 2005. Kaposi's sarcoma-associated herpesvirus modulates microtubule dynamics via RhoA-GTP-diaphanous 2 signaling and utilizes the dynein motors to deliver its DNA to the nucleus. *J. Virol.* 79:1191–1206. http://dx.doi.org/10.1128/JVI.79.2.1191-1206.2005

Pasdeloup, D., M. Labetoulle, and F.J. Rixon. 2013. Differing effects of herpes simplex virus 1 and pseudorabies virus infections on centrosomal function. *J. Virol.* 87:7102–7112. http://dx.doi.org/10.1128/JVI.00764-13

Perez, F., G.S. Diamantopoulos, R. Stalder, and T.E. Kreis. 1999. CLIP-170 highlights growing microtubule ends in vivo. *Cell.* 96:517–527. http://dx.doi.org/10.1016/S0092-8674(00)80656-X

Pierre, P., J. Scheel, J.E. Rickard, and T.E. Kreis. 1992. CLIP-170 links endocytic vesicles to microtubules. *Cell.* 70:887–900. http://dx.doi.org/10.1016/0092-8674(92)90240-D

Radtke, K., K. Döhner, and B. Sodeik. 2006. Viral interactions with the cytoskeleton: A hitchhiker's guide to the cell. *Cell. Microbiol.* 8:387–400. http://dx.doi.org/10.1111/j.1462-5822.2005.00679.x

Radtke, K., D. Kieneke, A. Wolfstein, K. Michael, W. Steffen, T. Scholz, A. Karger, and B. Sodeik. 2010. Plus- and minus-end directed microtubule motors bind simultaneously to herpes simplex virus capsids using different inner tegument structures. *PLoS Pathog.* 6:e1000991. http://dx.doi.org/10.1371/journal.ppat.1000991

Rickard, J.E., and T.E. Kreis. 1990. Identification of a novel nucleotide-sensitive microtubule-binding protein in HeLa cells. *J. Cell Biol.* 110:1623–1633. http://dx.doi.org/10.1083/jcb.110.5.1623

Roizman, B., D.M. Knipe, and R.J. Whitley. 2007. Herpes simplex viruses. *In* Fields Virology. Fifth edition. D.M. Knipe, P.M. Howley, et al., editors. Lipincott Williams and Wilkins, Philadelphia, PA. 2501–2602.

Roohvand, F., P. Maillard, J.P. Lavergne, S. Boulant, M. Walic, U. Andréo, L. Goueslain, F. Helle, A. Mallet, J. McLauchlan, and A. Budkowska. 2009. Initiation of hepatitis C virus infection requires the dynamic microtubule network: Role of the viral nucleocapsid protein. *J. Biol. Chem.* 284:13778–13791. http://dx.doi.org/10.1074/jbc.M807873200

Sabo, Y., D. Walsh, D.S. Barry, S. Tinaztepe, K. de Los Santos, S.P. Goff, G.G. Gundersen, and M.H. Naghavi. 2013. HIV-1 induces the formation of stable microtubules to enhance early infection. *Cell Host Microbe.* 14:535–546. http://dx.doi.org/10.1016/j.chom.2013.10.012

Skube, S.B., J.M. Chaverri, and H.V. Goodson. 2010. Effect of GFP tags on the localization of EB1 and EB1 fragments *in vivo*. *Cytoskeleton.* 67:1–12. http://dx.doi.org/10.1002/cm.20409

Slep, K.C., and R.D. Vale. 2007. Structural basis of microtubule plus end tracking by XMAP215, CLIP-170, and EB1. *Mol. Cell.* 27:976–991. http://dx.doi.org/10.1016/j.molcel.2007.07.023

Smith, G.A., L. Pomeranz, S.P. Gross, and L.W. Enquist. 2004. Local modulation of plus-end transport targets herpesvirus entry and egress in sensory axons. *Proc. Natl. Acad. Sci. USA.* 101:16034–16039. http://dx.doi.org/10.1073/pnas.0404686101

Sodeik, B., M.W. Ebersold, and A. Helenius. 1997. Microtubule-mediated transport of incoming herpes simplex virus 1 capsids to the nucleus. *J. Cell Biol.* 136:1007–1021. http://dx.doi.org/10.1083/jcb.136.5.1007

Stehbens, S.J., A.D. Paterson, M.S. Crampton, A.M. Shewan, C. Ferguson, A. Akhmanova, R.G. Parton, and A.S. Yap. 2006. Dynamic microtubules regulate the local concentration of E-cadherin at cell-cell contacts. *J. Cell Sci.* 119:1801–1811. http://dx.doi.org/10.1242/jcs.02903

Suomalainen, M., M.Y. Nakano, K. Boucke, S. Keller, and U.F. Greber. 2001. Adenovirus-activated PKA and p38/MAPK pathways boost microtubule-mediated nuclear targeting of virus. *EMBO J.* 20:1310–1319. http://dx.doi.org/10.1093/emboj/20.6.1310

Tai, C.Y., D.L. Dujardin, N.E. Faulkner, and R.B. Vallee. 2002. Role of dynein, dynactin, and CLIP-170 interactions in LIS1 kinetochore function. *J. Cell Biol.* 156:959–968. http://dx.doi.org/10.1083/jcb.200109046

Tripathy, S.K., S.J. Weil, C. Chen, P. Anand, R.B. Vallee, and S.P. Gross. 2014. Autoregulatory mechanism for dynactin control of processive and diffusive dynein transport. *Nat. Cell Biol.* 16:1192–1201. http://dx.doi.org/10.1038/ncb3063

Valetti, C., D.M. Wetzel, M. Schrader, M.J. Hasbani, S.R. Gill, T.E. Kreis, and T.A. Schroer. 1999. Role of dynactin in endocytic traffic: Effects of dynamitin overexpression and colocalization with CLIP-170. *Mol. Biol. Cell.* 10:4107–4120. http://dx.doi.org/10.1091/mbc.10.12.4107

Vallee, R.B., R.J. McKenney, and K.M. Ori-McKenney. 2012. Multiple modes of cytoplasmic dynein regulation. *Nat. Cell Biol.* 14:224–230. http://dx.doi.org/10.1038/ncb2420

Vaughan, K.T., S.H. Tynan, N.E. Faulkner, C.J. Echeverri, and R.B. Vallee. 1999. Colocalization of cytoplasmic dynein with dynactin and CLIP-170 at microtubule distal ends. *J. Cell Sci.* 112:1437–1447.

Vaughan, P.S., P. Miura, M. Henderson, B. Byrne, and K.T. Vaughan. 2002. A role for regulated binding of p150^{Glued}) to microtubule plus ends in organelle transport. *J. Cell Biol.* 158:305–319. http://dx.doi.org/10.1083/jcb.200201029

Walsh, D., and I. Mohr. 2004. Phosphorylation of eIF4E by Mnk-1 enhances HSV-1 translation and replication in quiescent cells. *Genes Dev.* 18:660–672. http://dx.doi.org/10.1101/gad.1185304

Watson, P., and D.J. Stephens. 2006. Microtubule plus-end loading of p150^{Glued} is mediated by EB1 and CLIP-170 but is not required for intracellular membrane traffic in mammalian cells. *J. Cell Sci.* 119:2758–2767. http://dx.doi.org/10.1242/jcs.02999

Weisbrich, A., S. Honnappa, R. Jaussi, O. Okhrimenko, D. Frey, I. Jelesarov, A. Akhmanova, and M.O. Steinmetz. 2007. Structure-function relationship of CAP-Gly domains. *Nat. Struct. Mol. Biol.* 14:959–967. http://dx.doi.org/10.1038/nsmb1291

Wolfstein, A., C.H. Nagel, K. Radtke, K. Döhner, V.J. Allan, and B. Sodeik. 2006. The inner tegument promotes herpes simplex virus capsid motility along microtubules *in vitro*. *Traffic.* 7:227–237. http://dx.doi.org/10.1111/j.1600-0854.2005.00379.x

Ye, G.J., K.T. Vaughan, R.B. Vallee, and B. Roizman. 2000. The herpes simplex virus 1 U_L34 protein interacts with a cytoplasmic dynein intermediate chain and targets nuclear membrane. *J. Virol.* 74:1355–1363. http://dx.doi.org/10.1128/JVI.74.3.1355-1363.2000

Zaichick, S.V., K.P. Bohannon, A. Hughes, P.J. Sollars, G.E. Pickard, and G.A. Smith. 2013. The herpesvirus VP1/2 protein is an effector of dynein-mediated capsid transport and neuroinvasion. *Cell Host Microbe.* 13:193–203. http://dx.doi.org/10.1016/j.chom.2013.01.009